Theoretical and Applied Mechanics Letters 6 (2016) 32–37

Contents lists available at ScienceDirect

Theoretical and Applied Mechanics Letters

journal homepage: www.elsevier.com/locate/taml

Review

Recent advances on thermal analysis of stretchable electronics

Yuhang Li [a], Yuyan Gao [b], Jizhou Song [b,c,*]

[a] Institute of Solid Mechanics, Beihang University (BUAA), Beijing 100191, China

[b] Department of Engineering Mechanics, Zhejiang University, Hangzhou 310027, China

[c] Soft Matter Research Center, Key Laboratory of Soft Machines and Smart Devices of Zhejiang Province, Zhejiang University, Hangzhou 310027, China

HIGHLIGHTS

- Recent advances on thermal analysis of stretchable electronics are overviewed.
- Scaling laws for the temperature increase in a constant and pulsed mode are established.
- Design guidelines for thermal management of stretchable electronics are provided.

ARTICLE INFO

Article history:
Received 16 October 2015
Received in revised form
2 December 2015
Accepted 16 December 2015
Available online 24 December 2015

Keywords:
Stretchable electronics
Thermal analysis
Scaling law

ABSTRACT

Stretchable electronics, which offers the performance of conventional wafer-based devices and mechanical properties of a rubber band, enables many novel applications that are not possible through conventional electronics due to its brittle nature. One effective strategy to realize stretchable electronics is to design the inorganic semiconductor material in a stretchable format on a compliant elastomeric substrate. Engineering thermal management is essential for the development of stretchable electronics to avoid adverse thermal effects on its performance as well as in applications involving human body and biological tissues where even 1–2 °C temperature increase is not allowed. This article reviews the recent advances in thermal management of stretchable inorganic electronics with focuses on the thermal models and their comparisons to experiments and finite element simulations.

Contents

1. Introduction

Fast developments and substantial achievements have been made on various aspects of stretchable electronics [1–7], which has superior mechanical properties that are inaccessible to conventional wafer-based electronics such as stretched like a rubber band and twisted like a rope without any significant reduction in electronic performance. Two complementary approaches have been demonstrated to develop stretchable electronics. One approach involves the use of the intrinsically compliant semiconductor materials to replace the intrinsically brittle inorganic semiconductor materials [8–11] that are widely used in conventional electronics. The other approach designs conventional high-performance inorganic semiconductor materials (e.g., Silicon) in a novel stretchable structure on a compliant substrate [12–15]. One such design is the bridge-island design with functional components residing on the island interconnected by the bridges to keep the islands almost un-

* Corresponding author at: Department of Engineering Mechanics, Zhejiang University, Hangzhou 310027, China.
E-mail address: jzsong@zju.edu.cn (J. Song).

http://dx.doi.org/10.1016/j.taml.2015.12.001

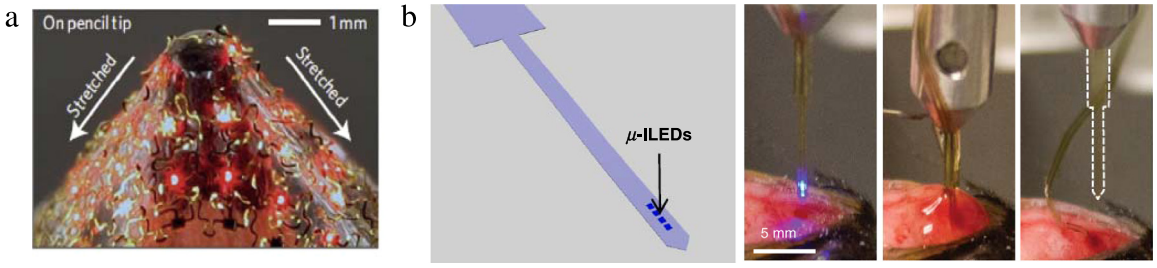

Fig. 1. (a) Stretchable inorganic light-emitting diodes with serpentine bridges, tightly stretched onto the sharp tip of a pencil. Reproduced with permission from Ref. [15]. Copyright 2010 Nature Publishing Group. (b) Scanning electron microscope (SEM) image of an injectable array of μ-ILEDs and the process of injection and release of the μ-ILEDs into the mouse brain for in vivo optogenetics. Reproduced with permission from Ref. [16]. Copyright 2013 AAAS.

deformed under stretching as shown in Fig. 1(a) of inorganic light-emitting diodes stretched onto the sharp tip of a pencil.

Thermal management of stretchable electronics is critically important because excessive heating may induce adverse responses such as the reduction of device performance and tissue lesioning (even 1–2 °C temperature increase) in applications (e.g., optogenetics, see Fig. 1(b)) involving biological tissues. The low conductivity ($\sim$0.1 W · m^{-1} · K^{-1}) of elastomeric substrate for stretchable electronics, which is about 3 orders lower than that of typical substrate for conventional electronics, imposes more challenges on the thermal management. This review paper will focus on the latter approach based on inorganic semiconductor materials and take microscale, inorganic light-emitting diodes (μ-ILEDs), which serve as heat sources and the active device islands in the bridge-island design for stretchable electronics, as an example to overview the recent advances in heat management of stretchable electronics through discussions of analytic, finite element simulations and experimental results.

2. Thermal analysis of μ-ILEDs under a constant power

Conventional design with individual packaged components interconnected by bulk wire bonding and mounted on a millimeter-scale heat sink for thermal management is not suitable for stretchable electronics, especially for applications of μ-ILEDs biology. Kim et al. [17] reported strategies using advanced methods in epitaxial liftoff and deterministic assembly and successfully fabricated μ-ILEDs on different substrates. Figure 2(a) shows the schematic diagram of the μ-ILED structure with the μ-ILED, encapsulated by benzocyclobutene (BCB) and metal layers, on the top of a glass substrate. Lu et al. [18] developed an analytic model by ignoring the structure details (e.g., p and n contacts) as shown in Fig. 2(b) to study the thermal properties of μ-ILEDs and establish a scaling law for the device temperature under a constant power. For simplicity, an axisymmetric model is adopted. The μ-ILED ($L \times L$) is modeled as a circular planar heat source with radius $r_0 = L/\sqrt{\pi}$ and the input power of Q at the BCB–glass interface. The comparison of surface temperature distributions in Fig. 2(c) from the analytical model, 3D finite element analysis (FEA) and experiments validates the analytical model. The μ-ILED temperature increase $\Delta T_{\mu\text{-ILED}} = T_{\mu\text{-ILED}} - T_0$ from the ambient temperature T_0 is given by

$$\begin{aligned}\Delta T_{\mu\text{-ILED}} &= \frac{2Q}{\pi k_B r_0^2}\int_0^\infty \beta(\xi) J_1^2(\xi r_0)\frac{\mathrm{d}\xi}{\xi^2} \\ &\approx 0.451\frac{Q}{k_g L}\left\{1 - 0.842\left(\frac{k_g L}{k_m H_m}\right)^{-1} \right. \\ &\quad \left. \times\left[1 - \exp\left(-1.07\frac{k_g L}{k_m H_m}\right)\right]\right\}, \end{aligned} \quad (1)$$

where k and H are the thermal conductivity and thickness with subscripts m, B and g for metal, BCB and the glass substrate, respectively, J_1 is the 1st-order Bessel function of the first kind and $\beta(\xi)$ is an analytic expression depending on material and geometry parameters [18]. The approximation in Eq. (1) holds for the facts that the glass thickness is much larger than other thickness ($H_g \gg H_m, H_B, r_0$), the thermal conductivity of metal is much larger than that of BCB ($k_m \gg k_B$), and the μ-ILED size is much larger than the metal and BCB layer thicknesses ($r_0 \gg H_m, H_B$). A simple scaling law could be easily established from Eq. (1): the normalized μ-ILED temperature $k_m H_m \left(T_{\mu\text{-ILED}} - T_0\right)/Q$ depends on only one non-dimensional parameter $k_g L/(k_m H_m)$. The scaling law (i.e., the approximate solution) agrees well with the accurate solution, 3D FEA and experiments in Fig. 2(d). It suggests that thick metal layer or large metal thermal conductivity help to reduce the μ-ILED temperature.

The temperature increase in Eq. (1) is for the single μ-ILED on a glass substrate and it can be easily extended to study other μ-ILED system with similar layouts and materials. Figure 3(a) shows the μ-ILED temperature as a function of μ-ILED size on a polyethylene terephthalate (PET) substrate at 160 mW · mm^2. The analytical prediction agrees very well with experiments. The temperature decreases with decreasing the μ-ILED size, which clearly indicates an effective route for thermal management: to divide a large LED to an array of μ-ILEDs. To find the temperature increase for μ-ILED array, the method of superposition can be used, i.e., $T_{\text{array}}(r,z) = T_0 + \sum_i \Delta T_i(r,z)$, where $\Delta T_i(r,z)$ is the temperature increase due to ith μ-ILED. The temperature increases for a conventional, macro-size LED (i.e., 0.5 × 0.5 mm^2), an array of 25 μ-ILEDs (i.e., 100 × 100 μm^2) at different spacings are shown in Fig. 3(b). The temperature of μ-ILED array decreases with increasing spacing and becomes independent of spacing for the spacing larger than $\sim$200 μm, which suggests a critical spacing to maximally reduce the temperature.

3. Thermal analysis of μ-ILEDs in a pulsed operation

In order to further decrease the device temperature, Kim et al. [19] applied a pulsed power and successfully fabricated μ-ILEDs on hydrogel substrate to simulate biological tissue. Figure 4(a) shows the layouts of a single μ-ILED on a polyimide (PI) layer attaching to a hydrogel substrate encapsulated by an epoxy (SU8) layer. Li et al. [20] developed an analytic model, validated by experiments and 3D FEA, to study the thermal properties of μ-ILED in a pulsed operation and derived a scaling law for the μ-ILED temperature increase. The PI layer and hydrogel substrate are taken as a single hydrogel layer (see Fig. 4(b)) since the PI layer has similar thermal properties as hydrogel. The pulsed power applied to the μ-ILED is defined by $Q(t) = Q_0 U(t)$ with Q_0 as the peak power and $U(t)$ as a unit pulsed power in Fig. 4(c). Let τ denote the pulse duration and t_0 the period of the pulse, the duty cycle D is defined by $D = \tau/t_0$. It is noted that under a pulsed power, the μ-ILED temperature first increases in a fluctuation way and then reached saturation

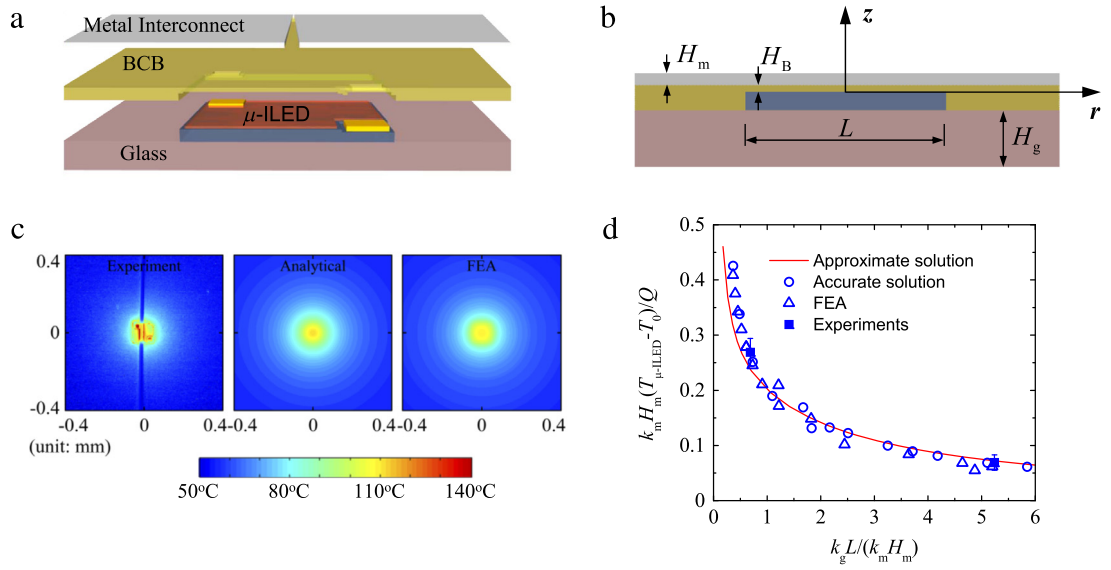

Fig. 2. Thermal management of μ-ILEDs on a glass substrate. (a) Three-dimensional illustrations of the μ-ILED structure. (b) A schematic illustration of the analytical model. (c) Surface temperature distribution given by experiments, analytical model and FEA for the input power $Q = 37.6$ mW with $L = 100$ μm. (d) The normalized μ-ILED temperature increase as the function of the normalized μ-ILED size for the approximate solution (solid line), accurate solution (circles), FEA (triangles) and experiments (squares). Reproduced with permission from Ref. [17]. Copyright 2012 The Royal Society.

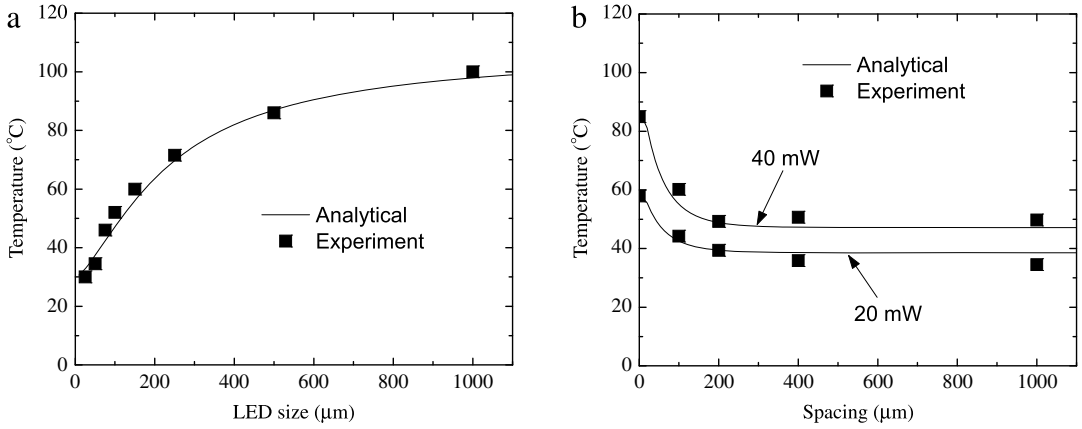

Fig. 3. Thermal management by controlling size and spatial distributions of μ-ILEDs on a PET substrate. (a) Measured (black symbols) and analytical predicted (black line) temperature as a function of μ-ILED size at 160 mW/mm^2. (b) Measured and (black symbols) and analytical predicted (black line) temperature of (5 × 5) μ-ILED array (100 × 100 μm^2) as a function of spacing. Reproduced with permission from Ref. [18]. Copyright 2012 Wiley-VCH Verlag GmbH&Co. KGaA, Weinheim.

$$\Delta T_{\mathrm{LED}}(t;\omega) = D\theta_{\mathrm{LED}}(0) + \sum_{n=1}^{\infty} |\theta_{\mathrm{LED}}(n\omega)| \left[\frac{\sin(2n\pi D)}{n\pi} \cos(n\omega t + \gamma_n) + \frac{1-\cos(2n\pi D)}{n\pi} \sin(n\omega t + \gamma_n) \right]$$

$$\approx \frac{Q_0}{\pi k_{\mathrm{sub}} r_0 \left(1 + \sqrt{\frac{k_{\mathrm{encap}} c_{\mathrm{encap}} \rho_{\mathrm{encap}}}{k_{\mathrm{sub}} c_{\mathrm{sub}} \rho_{\mathrm{sub}}}}\right)} \left\{ \frac{8D}{3\pi} + \sum_{n=1}^{\infty} \left[\left| \frac{\sqrt{\mathrm{i}r_0^2 n\omega/\alpha_{\mathrm{sub}}} - J_1\left(2\sqrt{\mathrm{i}r_0^2 n\omega/\alpha_{\mathrm{sub}}}\right) + L_1\left(2\sqrt{\mathrm{i}r_0^2 n\omega/\alpha_{\mathrm{sub}}}\right)}{\mathrm{i}r_0^2 n\omega/\alpha_{\mathrm{sub}}} \right| \cdot \left(\frac{\sin(2n\pi D)}{n\pi} \cos(n\omega t + \delta_n) + \frac{1-\cos(2n\pi D)}{n\pi} \sin(n\omega t + \delta_n) \right) \right] \right\} \quad (2)$$

Box I.

in a constant band after a few seconds (see Fig. 4(d)). The periodic pulsed power can be expressed via its Fourier series by $Q(t) = Q_0 \left(a_0 + \sum_{n=1}^{\infty} a_n \cos n\omega t + \sum_{n=1}^{\infty} b_n \sin n\omega t\right)$, where $\omega = 2\pi/t_0$, $a_0 = D = \tau/t_0$, $a_n = \sin(2n\pi D)/(n\pi)$, and $b_n = [1-\cos(2n\pi D)]/(n\pi)$. The temperature increase after saturation could be obtained analytically by the superposition of

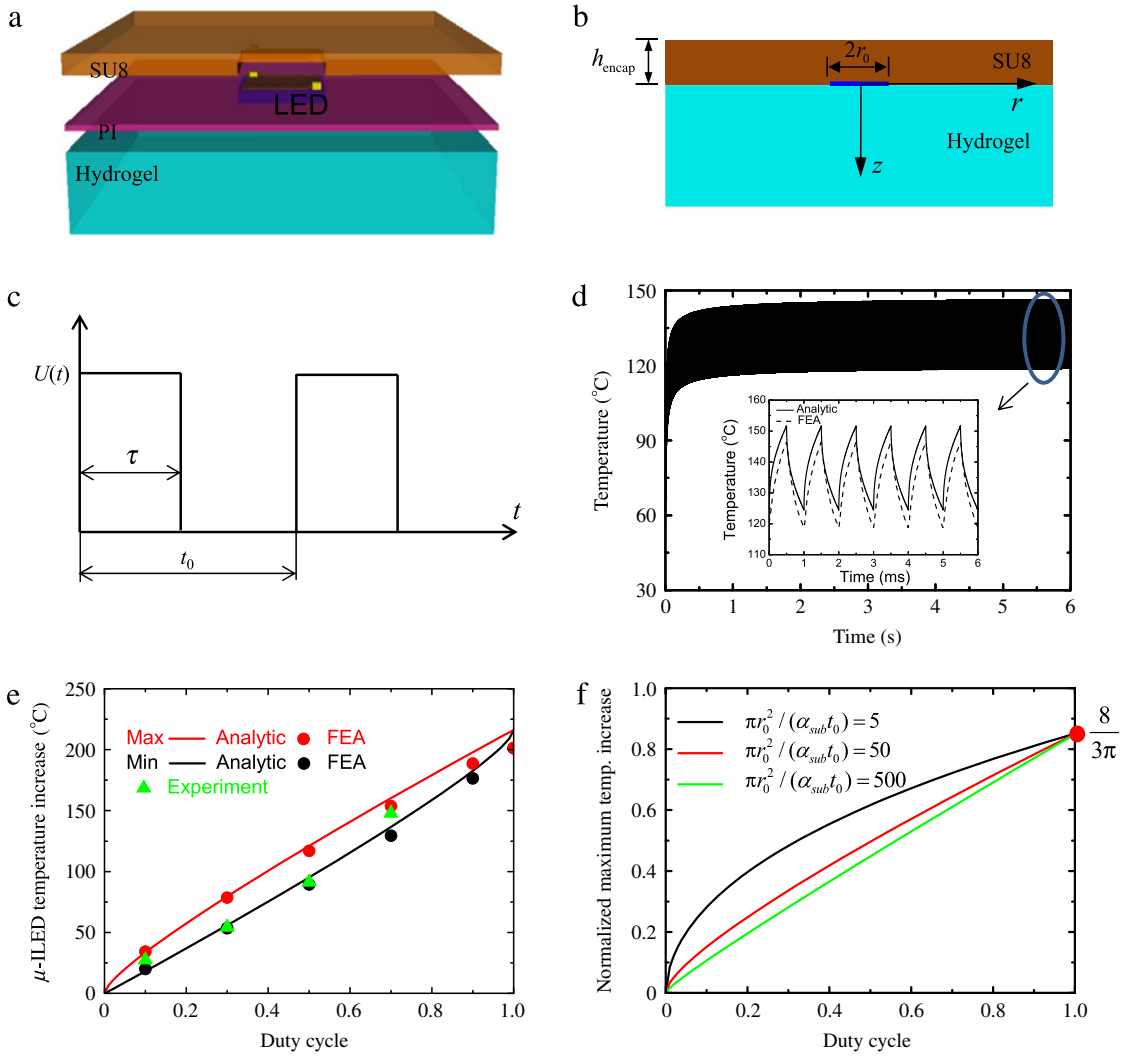

Fig. 4. (a) Three-dimensional illustration of the μ-ILED on a hydrogel substrate. (b) A schematic illustration of the analytical model. (c) A unit pulsed power with duration time τ and period t_0. (d) Temperature for the pulsed peak power 20 mW with $D = 50\%$ and $t_0 = 1$ ms with the inset as the temperature after saturation. (e) The maximum and minimum μ-ILED temperature increase as the function of the duty cycle for the peak power 30 mW with $t_0 = 1$ ms. (f) The normalized maximum μ-ILED temperature increase at a pulsed power as the function of the duty cycle. Reproduced with permission from Ref. [19]. Copyright 2013 American Institute of Physics.

the solution due to a sinusoidal power $Q_0 \cos(\omega t)$ [or $Q_0 \sin(\omega t)$], which can be written as the real (or imaginary) part of $Q_0 e^{i\omega t}$, and is given by Eq. (2) in Box I where γ_n is the phase angle of $\theta_{LED}(n\omega) = \frac{2Q_0}{\pi r_0^2}\int_0^\infty f(\xi)\frac{J_1^2(\xi r_0)}{\xi}\cosh\left(h_{encap}\sqrt{\xi^2+iq_{encap}^2}\right)d\xi$, which is the temperature increase due to a power of $Q_0 e^{i\omega t}$, δ_n is the phase angle of $\left[\sqrt{ir_0^2\omega/\alpha_{sub}} - J_1\left(2\sqrt{ir_0^2\omega/\alpha_{sub}}\right) + L_1\left(2\sqrt{ir_0^2\omega/\alpha_{sub}}\right)\right]/\left(ir_0^2\omega/\alpha_{sub}\right)$, L_1 is the 1st-order modified Struve function, and $f(\xi)$ is an analytic expression depending on material and geometry parameters [20]. $r_0 = L/\sqrt{\pi}$, h is the thickness, and $q = \sqrt{n\omega/\alpha}$ with $\alpha = k/(c\rho)$ as the thermal diffusivity, where k is the thermal conductivity, c is the specific heat capacity, and ρ is the mass density. The subscripts "encap" and "sub" denote the SU8 encapsulation and hydrogel substrate, respectively. The approximation in Eq. (2) holds for the facts that $\sqrt{\omega/\alpha_{encap}}$ is usually larger, or on the order of, a few μm^{-1} for polymer with period less than 1 ms as in applications of optogenetics, and h_{encap} is larger than, or on the order of, a few μm.

The good agreement between the analytical predictions from Eq. (2) and FEA for the temperature after saturation for $L = 100$ μm, $Q_0 = 30$ mW, $D = 50\%$ and $t_0 = 1.0$ ms in the inset of Fig. 4(d) validates the analytical model. The constant band for the temperature increase after saturation defines the maximum and minimum temperature. Figure 4(e) shows the dependence of the maximum and minimum temperature increase of μ-ILED on the duty cycle. The analytical model agrees well with FEA, and the experimental measurements are indeed within the minimum and maximum temperature increase predicted by the analytical model. It is shown that a smaller duty cycle could effectively decrease the μ-ILED temperature, which suggests that μ-ILEDs could be operated in a pulsed mode but with a much lower temperature increase compared to that in a constant mode. Eq. (2) also indicates that the normalized maximum temperature increase $\left(1+\sqrt{\frac{k_{encap}c_{encap}\rho_{encap}}{k_{sub}c_{sub}\rho_{sub}}}\right)\frac{\pi k_{sub}r_0}{Q_0}\Delta T_{LED}^{max}$ only depends on two non-dimensional parameters: D and $\pi r_0^2/(\alpha_{sub}t_0)$. This simple scaling law is illustrated in Fig. 4(f). It is shown that small duty cycle D or large $\pi r_0^2/(\alpha_{sub}t_0)$ helps to reduce the maximum temperature of μ-ILEDs. For large $\pi r_0^2/(\alpha_{sub}t_0) \gg 1$, the maximum temperature increase in μ-ILED is approximately linear with D, and is given by

$$\Delta T_{LED}^{max} \approx \frac{0.48Q_0}{k_{sub}\sqrt{\pi r_0^2}}\frac{D}{1+\sqrt{\frac{k_{encap}c_{encap}\rho_{encap}}{k_{sub}c_{sub}\rho_{sub}}}} \quad \text{for} \quad \frac{\pi r_0^2}{\alpha_{sub}t_0} \gg 1. \qquad (3)$$

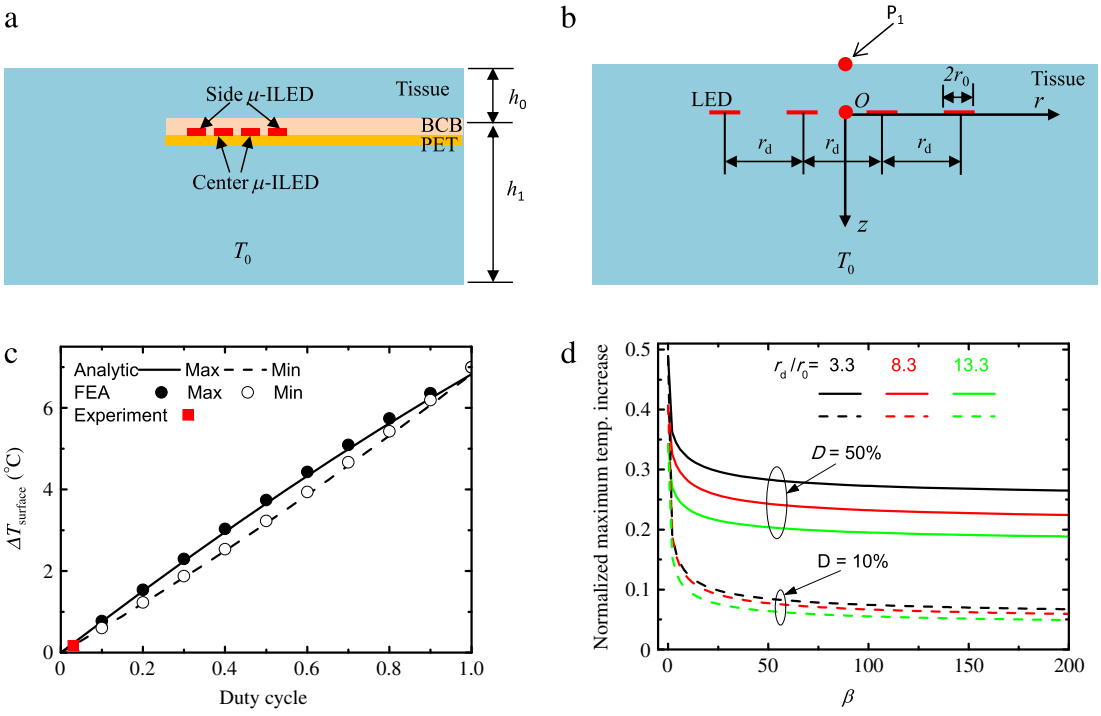

Fig. 5. (a) Cross-sectional illustration of four μ-ILEDs in biological tissue. (b) A schematic illustration of the analytical model. (c) Surface temperature increase determined by analytical model, FEA, and experiments as the function of duty cycle with the frequency 3 Hz, peak power $Q_0 = 2.5$ mW, $r_0 = 60$ μm, $r_d = 200$ μm, $h_0 = 0.3$ mm, and $h_1 = 3.7$ mm. (d) Maximum normalized temperature increase of center μ-ILED as the function of the normalized parameter. Reproduced with permission from Ref. [20]. Copyright 2013 The Royal Society.

4. Thermal analysis of μ-ILEDs in optogenetics

Li et al. [21] further extended the above model to perform thermal management of μ-ILEDs in optogenetics. Kim et al. [21] developed injectable, wireless optoelectronic devices with μ-ILED arrays delivered into the mouse brain using a releasable microneedle for in vivo optogenetics. Figure 5(a) schematically shows the cross-section of four μ-ILEDs coated with a thin (6 μm) layer of benzocyclobutene (BCB) on a 2.5 μm thick polyethylene terephthalate (PET) substrate in an explanted piece of tissue from the mouse brain with the dimension of $9 \times 4 \times 4$ mm^3 held at $T_0 =$ 37 °C by a thermal stage. h_0 and h_1 denote the tissue thicknesses above and below the μ-ILEDs, respectively. The thermal properties of BCB and PET are similar to those of tissue, and therefore their effects on the temperature are neglected. Li et al. [21] developed an analytical model for μ-ILED arrays in a pulsed operation in biological tissues and established a simple scaling law for the maximum temperature increase in terms of material, geometric and loading parameters. An array of 4 μ-ILEDs used in experiments [16] is taken as an example to illustrate the approach.

Figure 5(b) shows a schematic illustration of the analytical model for 4 μ-ILEDs in the tissue with a pulsed power $Q(t) = Q_0 U(t)$ applied to a single μ-ILED. Let r_d denote the distance between the centers of two adjacent μ-ILEDs. With the origin at the center of arrays, the coordinates of μ-ILED centers are $(\pm 3r_d/2, 0)$ and $(\pm r_d/2, 0)$, respectively. Following the similar approach as the one for μ-ILED on a hydrogel substrate [20], the temperature increase for a single μ-ILED in biological tissue is obtained first and then the method of superposition is used to obtain the temperature increase for the μ-ILED array. Let $\theta(r, z; \omega)$ denote the temperature increase for a single μ-ILED due to a sinusoidal power $Q_0 \cos(\omega t)$ [or $Q_0 \sin(\omega t)$]. The temperature increase at the center point P_1 of the top surface due to a sinusoidal power is obtained as $\theta_{surface}(\omega) = 2\theta(r = r_d/2, z = -h_0; \omega) + 2\theta(r = 3r_d/2, z = -h_0; \omega)$. The temperature increase at the center point P_1 of the top surface due to the pulsed power is then obtained as

$$\Delta T_{surface}(t; \omega) = D\theta_{surface}(0) + \sum_{n=1}^{\infty} |\theta_{surface}(n\omega)| \times \left[\frac{\sin(2n\pi D)}{n\pi} \cos(n\omega t + \zeta_n) + \frac{1 - \cos(2n\pi D)}{n\pi} \sin(n\omega t + \zeta_n) \right], \quad (4)$$

where ζ_n is the phase angle of $\theta_{surface}(n\omega)$ with the expression that can found in Ref. [21]. Figure 5(c) compares the maximum and minimum temperature increase after saturation from Eq. (4), 3D FEA and experiments for the frequency 3 Hz, peak power $Q_0 = 2.5$ mW, $r_0 = 60$ μm, $r_d = 200$ μm, $h_0 = 0.3$ mm, and $h_1 = 3.7$ mm. The good agreement indicates that the analytical model could predict the temperature distributions accurately.

The maximum temperature increase in the array of four μ-ILEDs occurs at the center μ-ILED. For large ratios of h_0/r_0 and h_1/r_0 as in experiments [21], the analytical model gives the normalized temperature increase of the center μ-ILED as in Box II, where E is the complete elliptic integral of the second kind, $\beta = A/(\alpha t_0)$ with $A(=2\pi r_0^2)$ as the total surface area of μ-ILED, J_0 is 0th-order Bessel function of the first kind, and η_n is the phase angle of $\int_0^\infty \frac{J_1(\xi)}{\sqrt{\xi^2 + i \cdot n\beta}} \left[\frac{J_1(\xi)}{\xi} + J_0\left(\frac{\sqrt{2\pi} r_d}{\sqrt{A}} \xi\right) + \frac{1}{2} J_0\left(\frac{2\sqrt{2\pi} r_d}{\sqrt{A}} \xi\right) \right] d\xi$. Eq. (5) shows a simple scaling law for the normalized maximum temperature increase $\Delta T^{max}_{center\ LED} / \left[Q_0 / \left(k\sqrt{A} \right) \right]$ as shown in Fig. 5(d), which only depends on three non-dimensional parameters: $r_d/\sqrt{A}$, β and D. The normalized maximum temperature increase of the center μ-ILED drops significantly for $0 < \beta < 40$ and then remains almost unchanged for $\beta > 40$. The results show that large $r_d/\sqrt{A}$, small β and D help to reduce the maximum temperature increase. The above results for μ-ILEDs in a constant or pulsed operation are applied to optimize the injectable optoelectronics to

$$\frac{\Delta T_{\text{center LED}}(t)}{Q_0\Big/\left(k\sqrt{A}\right)} = \sqrt{\frac{2}{\pi^3}}D\left[\frac{4}{3}+2E\left(\sqrt{2\pi}\frac{r_\mathrm{d}}{\sqrt{A}}\right)+E\left(2\sqrt{2\pi}\frac{r_\mathrm{d}}{\sqrt{A}}\right)\right] + \sqrt{\frac{2}{\pi}}\sum_{n=1}^{\infty}\left\{\left|\int_0^\infty \frac{J_1(\xi)}{\sqrt{\xi^2+\mathrm{i}\cdot n\beta}}\left[\frac{J_1(\xi)}{\xi}+J_0\left(\frac{\sqrt{2\pi}r_\mathrm{d}}{\sqrt{A}}\xi\right)+\frac{1}{2}J_0\left(\frac{2\sqrt{2\pi}r_\mathrm{d}}{\sqrt{A}}\xi\right)\right]\mathrm{d}\xi\right|\cdot \left[\frac{\sin(2n\pi D)}{n\pi}\cos\left(\frac{2\pi nt}{t_0}+\eta_n\right)+\frac{1-\cos(2n\pi D)}{n\pi}\sin\left(\frac{2\pi nt}{t_0}+\eta_n\right)\right]\right\} \tag{5}$$

Box II.

maintain the temperature low enough to avoid tissue lesioning for in vivo optoelectronics [16].

5. Summary

In summary, with fast developments and substantial achievements made on various aspects of stretchable electronics, thermal management of stretchable electronics becomes more and more important due to its adverse effects on its performance as well as in applications involving human body, where even a small temperature increase (1–2 °C) is not allowed. This paper overviews the recent advances on thermal analysis of stretchable inorganic electronics and provides design guidelines for thermal management (e.g., to use small functional components in a pulsed mode). While several efforts have been devoted to develop analytical models with certain assumptions, there are still many open challenges and opportunities for future research. For example, a biophysically realistic model, which accounts for the effects of blood perfusion and metabolic heat generation, is needed and remain an attracting area of research. Such a model will help researchers to optimally design experiment and offer the possibility of direct integration of stretchable electronics and optoelectronics with biological tissues for emerging applications.

Acknowledgments

This work was supported by the Zhejiang Provincial Natural Science Foundation of China (Grant No. LR15A020001), the National Natural Science Foundation of China (Grant Nos. 11502009, 11372272 and 11321202), and the National Basic Research Program of China (Grant No. 2015CB351900).

References

[1] D.H. Kim, J.H. Ahn, W.M. Choi, et al., Stretchable and foldable silicon integrated circuits, Science 320 (2008) 507–511.
[2] J. Viventi, D.H. Kim, L. Vigeland, et al., Flexible, foldable, actively multiplexed, high-density electrode array for mapping brain activity in vivo, Nature Neurosci. 14 (2011) 1599–1605.
[3] D.H. Kim, R. Ghaffari, N. Lu, et al., Flexible and stretchable electronics for biointegrated devices, Annu. Rev. Biomed. Eng. 14 (2012) 113–128.
[4] H.C. Ko, M.P. Stoykovich, J. Song, et al., A hemispherical electronic eye camera based on compressible silicon optoelectronics, Nature 454 (2008) 748–753.
[5] R.C. Webb, A.P. Bonifas, A. Behnaz, et al., Ultrathin conformal devices for precise and continuous thermal characterization of human skin, Nature Mater. 12 (2013) 938–944.
[6] S. Xu, Y. Zhang, L. Jia, et al., Soft microfluidic assemblies of sensors, circuits, and radios for the skin, Science 344 (2014) 70–74.
[7] C. Dagdeviren, B.D. Yang, Y. Su, et al., Conformal piezoelectric energy harvesting and storage from motions of the heart, lung, and diaphragm, Proc. Natl. Acad. Sci. USA 111 (2014) 1927–1932.
[8] B. Crone, A. Dodabalapur, Y.Y. Lin, et al., Large-scale complementary integrated circuits based on organic transistors, Nature 403 (2000) 521–523.
[9] Y.L. Loo, T. Someya, K.W. Baldwin, et al., Soft, conformable electrical contacts for organic semiconductors: high-resolution plastic circuits by lamination, Proc. Natl. Acad. Sci. USA 99 (2002) 10252–10256.
[10] T. Sekitani, T. Yokota, U. Zschieschang, et al., Organic nonvolatile memory transistors for flexible sensor arrays, Science 326 (2009) 1516–1519.
[11] M. Kaltenbrunner, T. Sekitani, J. Reeder, et al., An ultra-lightweight design for imperceptible plastic electronics, Nature 499 (2013) 458–463.
[12] H. Jiang, D.Y. Khang, J. Song, et al., Finite deformation mechanics in buckled thin films on compliant supports, Proc. Natl. Acad. Sci. USA 104 (2007) 15607–15612.
[13] D.H. Kim, J. Song, W.M. Choi, et al., Materials and noncoplanar mesh designs for integrated circuits with linear elastic responses to extreme mechanical deformations, Proc. Natl. Acad. Sci. USA 105 (2008) 18675–18680.
[14] S. Xu, Y. Zhang, J. Cho, et al., Stretchable batteries with self-similar serpentine interconnects and integrated wireless recharging systems, Nature Commun. 4 (2013) 1543.
[15] R.H. Kim, D.H. Kim, J. Xiao, et al., Waterproof AlInGaP optoelectronics on stretchable substrates with applications in biomedicine and robotics, Nature Mater. 9 (2010) 929–937.
[16] T. Kim, J.G. McCall, Y.H. Jung, et al., Injectable, cellular-scale optoelectronics with applications for wireless optogenetics, Science 340 (2013) 211–216.
[17] H.S. Kim, E. Brueckner, J. Song, et al., Unusual strategies for using indium gallium nitride grown on silicon (111) for solid-state lighting, Proc. Natl. Acad. Sci. USA 108 (2011) 10072–10077.
[18] C. Lu, Y. Li, J. Song, et al., A thermal analysis of the operation of microscale, inorganic light-emitting diodes, Proc. R. Soc. Lond. Ser. A Math. Phys. Eng. Sci. 468 (2012) 3215–3223.
[19] T. Kim, Y.H. Jung, J. Song, et al., High-efficiency, microscale GaN light-emitting diodes and their thermal properties on unusual substrates, Small 8 (2012) 1643–1649.
[20] Y. Li, Y. Shi, J. Song, et al., Thermal properties of microscale inorganic light-emitting diodes in a pulsed operation, J. Appl. Phys. 113 (2013) 144505.
[21] Y. Li, X. Shi, J. Song, et al., Thermal analysis of injectable, cellular-scale optoelectronics with pulsed power, Proc. R. Soc. Lond. Ser. A Math. Phys. Eng. Sci. 469 (2013) 20130142.